An Assessment of Theoretical Procedures for Predicting the Thermochemistry and Kinetics of Hydrogen Abstraction by Methyl Radical from Benzene

Karen Hemelsoet,[†,‡] Damian Moran,[*,‡] Veronique Van Speybroeck,[*,†] Michel Waroquier,[†] and Leo Radom[*,‡]

Center for Molecular Modeling, Ghent University, Proeftuinstraat 86, B-9000 Gent, Belgium, and School of Chemistry and ARC Centre of Excellence in Free Radical Chemistry and Biotechnology, University of Sydney, Sydney, NSW 2006, Australia

Received: March 23, 2006; In Final Form: May 13, 2006

The reaction enthalpy (298 K), barrier (0 K), and activation energy and preexponential factor (600−800 K) have been examined computationally for the abstraction of hydrogen from benzene by the methyl radical, to assess their sensitivity to the applied level of theory. The computational methods considered include high-level composite procedures, including W1, G3-RAD, G3(MP2)-RAD, and CBS-QB3, as well as conventional ab initio and density functional theory (DFT) methods, with the latter two classes employing the 6-31G(d), 6-31+G(d,p) and/or 6-311+G(3df,2p) basis sets, and including ZPVE/thermal corrections obtained from 6-31G(d) or 6-31+G(d,p) calculations. Virtually all the theoretical procedures except UMP2 are found to give geometries that are suitable for subsequent calculation of the reaction enthalpy and barrier. For the reaction enthalpy, W1, G3-RAD, and URCCSD(T) give best agreement with experiment, while the large-basis-set DFT procedures slightly underestimate the endothermicity. The reaction barrier is slightly more sensitive to the choice of basis set and/or correlation level, with URCCSD(T) and the low-cost BMK method providing values in close agreement with the benchmark G3-RAD value. Inspection of the theoretically calculated rate parameters reveals a minor dependence on the level of theory for the preexponential factor. There is more sensitivity for the activation energy, with a reasonable agreement with experiment being obtained for the G3 methods and the hybrid functionals BMK, BB1K, and MPW1K, especially in combination with the 6-311+G(3df,2p) basis set. Overall, the high-level G3-RAD composite procedure, URCCSD(T), and the cost-effective DFT methods BMK, BB1K, and MPW1K give the best results among the methods assessed for calculating the thermochemistry and kinetics of hydrogen abstraction by the methyl radical from benzene.

1. Introduction

Hydrogen-abstraction reactions are ubiquitous in chemistry and biology and have been studied in such diverse areas as cosmology, combustion science, and the polymer industry. For example, the initiation step in coke formation,[1] an industrially important side process of thermal hydrocarbon cracking, is hydrogen abstraction.[2−4] To model these potentially complex reaction processes, calculations on some of the contributing elementary reactions are advisable, as they provide the opportunity to obtain the required levels of insight and understanding for model genesis.[5−8] In the present paper, we will focus on the abstraction of hydrogen from benzene by the methyl radical (see Figure 1), as this represents a fundamental point of comparison for radical-mediated hydrogen abstractions from the benzenoid components of polycyclic aromatic hydrocarbons (PAHs).[9,10] PAHs are of general interest, as some are known carcinogens,[11] and they are formed as byproducts during the incomplete combustion of organic substances such as coal, oil, and waste.[12−15] Of related relevance to radical-abstraction reactions are radical-addition processes,[16−18] where a delicate balance between the various factors governing reaction kinetics and thermochemistry has been demonstrated both experimentally and theoretically.[19]

Hydrogen-abstraction reactions have been the subject of numerous computational studies.[2,20−23] Of most relevance to the present investigation is the comprehensive work of Tokmakov et al.,[22] who examined the reaction of phenyl radical with methane (i.e., the reverse of the reaction of benzene plus methyl radical) at the G2M(CC,MP2) level of theory and reported an exothermicity at 0 K of 43.1 kJ mol^{-1} and a barrier of 38.8 kJ mol^{-1} for the process. Their predicted G2M(CC,MP2) exothermicity is approximately 6.3 kJ mol^{-1} greater than experiment, which they attributed[22] to the highly spin-contaminated unrestricted wave function of the phenyl radical[24,25] (leading to the energy of the phenyl radical being overestimated). Also of interest is the recent assessment study by Coote,[23] who found MPW1K/6-311+G(3df,2p) to be a reliable, yet cost-effective, theoretical method for modeling the hydrogen-abstraction reactions of carbon-centered radicals. In a related radical study,[17] we found that the geometries, frequency factors, and temperature corrections for a series of radical-addition reactions to C=C and C≡C bonds were relatively insensitive to the level of theory, while reaction enthalpies and barrier heights were very sensitive to the method employed.[17] As the aromatic ring might have a substantial influence on these quantities, the conclusions

* Authors to whom correspondence should be addressed. E-mail: dmoran@chem.usyd.edu.au; veronique.vanspeybroeck@ugent.be; radom@chem.usyd.edu.au.
† Ghent University.
‡ University of Sydney.

10.1021/jp061823z CCC: $33.50
Published on Web 06/29/2006

obtained from these previous studies on radical reactions involving nonaromatic species might not necessarily be applicable to the present investigation.

For the reaction of benzene with the methyl radical ($C_6H_6 + \bullet CH_3 \rightarrow \bullet C_6H_5 + CH_4$), relevant data from two experiments are available.[26,27] Using a flow-tube experiment with either dimethylmercury or dimethylcadmium as the $\bullet CH_3$ source, Krech and Price[26] measured a rate constant of $k(T) = 6.3 \times 10^4\ e^{(-4680/T)}\ m^3\ mol^{-1}\ s^{-1}$ within the temperature range 744−800 K. More recently, Zhang et al.[27] conducted a steady-state analysis of CH_4 formation during pyrolysis of C_2H_4 in the presence of C_6H_6 at temperatures of 650−770 K, leading to a rate constant $k(T) = 2.0 \times 10^6\ e^{(-7580/T)}\ m^3\ mol^{-1}\ s^{-1}$. However, both the slope and the intercept for $1/T \rightarrow 0$ of the rate curves in these two experiments show substantial differences, and therefore, so do the activation energies and the preexponential factors. These differences may at least partly be associated with the narrow temperature ranges used for the extrapolations.

As noted above, the reverse of the benzene abstraction reaction, i.e., $CH_4 + \bullet C_6H_5 \rightarrow \bullet CH_3 + C_6H_6$, has been examined experimentally by Tokmakov et al.,[22] who used the complementary methods of pyrolysis/Fourier transform IR spectroscopy and pulsed-laser-photolysis/mass spectrometry. They reported a rate constant $k(T)$ for this process of $6.0 \times 10^6\ e^{(-6201/T)}\ m^3\ mol^{-1}\ s^{-1}$ in the temperature range 600−980 K. They also noted the disparity between the kinetic parameters reported by Krech and Price[26] and Zhang et al.[27] Other experimental data for the reverse of the benzene abstraction reaction have been obtained by Heckmann et al.[28] and Duncan et al.[29]

In recent years, there has been significant testing of a wide range of theoretical procedures for their ability to obtain reliable and accurate reaction thermochemistry and kinetics. Density functional theory (DFT) methods have often been found to provide an excellent cost-to-reliability performance and have therefore seen increased popularity.[30] B3-LYP is undoubtedly the most widely used DFT functional,[31] but its limitations—including the troublesome description of unstable structures such as transition structures (TSs), especially when polar effects are important—are also potentially problematic for hydrogen-abstraction reactions.[2,21,23,32,33] Recent studies on benchmark systems have shown that the new hybrid metafunctionals such as BMK,[34] MPWB1K,[35] and TPSS1KCIS[36] perform better than B3-LYP in certain situations.[37]

The main goal of the current work is to examine the influence of level of theory on optimized geometries, reaction enthalpies at 298 K (ΔH_{298}), barriers ($\Delta E_0^{\ddagger}$), activation energies (E_a), preexponential factors (A), and rate constants (k) for the abstraction of hydrogen from benzene by the methyl radical. This study will serve as a reference for further work on larger polyaromatic systems, and in this respect, we will focus particularly on identifying accurate and yet affordable computational methods that might be suitable for modeling the hydrogen-abstraction reactions of a broad variety of benzenoid hydrocarbons. As part of the study, the influence of level of theory on rate constants is also investigated, and comparison is made with experimental data. Although the characteristics and reactive behavior of benzene and other PAHs[3,8,10] have been previously investigated, this study represents the first systematic assessment of the performance of theory for calculating the thermochemical and kinetic properties of the hydrogen-abstraction reaction between benzene and the methyl radical.

2. Theoretical Procedures

Molecular orbital theory[38] and density functional theory (DFT)[39] calculations were performed using the *Gaussian 03*,[40] *Molpro 2000.6*,[41] and *ACES II*[42] program packages. Unless noted otherwise, calculations on radicals were performed with an unrestricted open-shell wave function. The "U" prefix is often omitted, though it is sometimes included for emphasis. In the limited number of cases where a restricted open-shell wave function was used, this is indicated by an "R" prefix. The frozen-core approximation was used throughout, except where full calculations were required as part of a standard composite method.

Geometries were optimized at the BP86, BLYP, B3-P86, B3-LYP, B3-PW91, MPW1K, BB1K, MPWB1K, BMK, UHF, RHF, UMP2, UQCISD, and UCCSD levels of theory, in conjunction with the 6-31G(d) and 6-31+G(d,p) basis sets. The B3-LYP and CCSD methods were also used in combination with the 6-31G(d,p) and/or 6-311G(d,p) basis sets. Harmonic vibrational frequencies were computed at the same level of theory as the geometry optimization and used (after appropriate scaling) to provide zero-point vibrational energies (ZPVEs) and to confirm the nature of the stationary points. Single-point energy calculations were performed for each geometry at the URCCSD(T)/6-311+G(d,p) level, with the calculated total energies allowing the quality of the optimized structures to be evaluated.

Using the B3-LYP/6-31+G(d,p) and BMK/6-31+G(d,p) optimized geometries, hydrogen-abstraction barriers and reaction enthalpies were computed using a variety of standard DFT methods in combination with the 6-31G(d) and 6-31+G(d,p) basis sets. In addition to these small-basis-set calculations, UB3-LYP, RB3-LYP, B3-PW91, MPW1PW91, MPW1K, BB1K, MPWB1K, BMK, UHF, RHF, UMP2, RMP2, and the UR-CCSD(T) procedure of Molpro were also used with the 6-311+G(3df,2p) basis set. The barriers and reaction enthalpies were also computed with the CBS-QB3,[43] G3(MP2)-RAD,[44] and G3-RAD[45] high-level composite procedures. The reaction enthalpy was also computed with the W1 procedure,[46] which has been found, when evaluated with a large test set of thermochemical data, to generally give agreement with experiment to within 2 kJ mol^{-1}.[46]

We applied transition state theory (TST)[47] to calculate the rate constants using the expression[48]

$$k(T) = \kappa \frac{k_B T}{h} \frac{q_{\ddagger}/V}{(q_A/V)(q_B/V)} e^{-(\Delta E_0^{\ddagger}/k_B T)} \qquad (1)$$

where κ is the tunneling coefficient, k_B is the Boltzmann constant, h is Planck's constant, V is the reference volume in which the translational part of the partition function is evaluated, q_A, q_B, and $q_{\ddagger}$ relate to the molecular partition functions of the reactants (A and B) and transition structure (TS), respectively, and $\Delta E_0^{\ddagger}$ is the ZPVE-corrected energy difference between the TS and the reactants (i.e., the reaction barrier) at 0 K. To calculate the tunneling coefficient, κ, the Wigner[49] and Eckart[50] methods were tested, representing simple procedures that only need to consider the reaction stationary points and are therefore compatible with TST. In general, the Eckart method is considered to be superior to the Wigner approximation,[51] as the latter depends solely on the imaginary frequency of the TS and can grossly underestimate the effect of tunneling. The Eckart approximation, on the other hand, is found often to overestimate the tunneling contribution, especially at very low temperature.[51]

The link with the macroscopic quantities found in the Arrhenius rate law is made by a linear fit to a set of $k(T)$ values calculated using eq 1 for a range of temperatures. One refinement in our theoretical treatment comes from the observa-

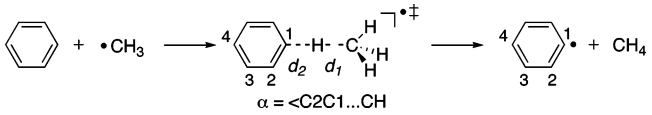

Figure 1. Hydrogen abstraction from benzene by the methyl radical to form the phenyl radical plus methane. The forming bond length (d_1), breaking bond length (d_2), and torsional angle (α) of the transition structure are highlighted.

tion that the TS of the reaction between benzene and methyl radical has a very-low-frequency vibration, corresponding to internal rotation of the methyl group about the forming bond. As a result, the free rotor (FR) approximation is used to model this mode.[52] In a recent study on radical-addition reactions, we demonstrated the importance of correctly describing hindered internal rotations in order to obtain reliable partition functions.[6,53] In the present case, we use a mixed harmonic oscillator/free rotor (HO/FR) model, in which all the internal motions except for the methyl torsion in the TS are approximated as independent harmonic oscillators and the corresponding partition functions are obtained as a product of contributions of the form

$$q_{\mathrm{vib},i} = \frac{\mathrm{e}^{-(h\nu_i/2k_\mathrm{B}T)}}{1-\mathrm{e}^{-(h\nu_i/k_\mathrm{B}T)}} \qquad (2)$$

for each of the internal modes i ($i = 1, ..., 3N - 6$ for a nonlinear molecule). For the internal motion of the methyl group in the TS, the standard HO contribution is replaced by a manually constructed FR partition function given by

$$q_{\mathrm{FR}} = \frac{1}{\sigma_{\mathrm{int}}}\sqrt{\frac{k_\mathrm{B}T\pi}{h\nu}} = \frac{1}{\sigma_{\mathrm{int}}}\sqrt{\frac{2k_\mathrm{B}T\pi I_\mathrm{m}}{\hbar^2}} \qquad (3)$$

where σ_{int} is the symmetry number, and I_m is the reduced moment of inertia.

Another important consideration for an accurate description of reaction kinetics and thermochemistry is the use of ZPVE and thermal-correction scaling factors,[54] as they provide a means for accounting for systematic deviations between measured and computed frequency-dependent properties.[21,36,54−56] Published scaling factors for the thermal correction to the enthalpy are not available for the hybrid meta-DFT functionals, and a value of 0.98 is used.

3. Results and Discussion

3.1. Geometries. The hydrogen abstraction from benzene by a methyl radical to form the phenyl radical plus methane is shown in Figure 1. Three of the geometric parameters vary significantly during the course of the reaction. These are the forming (d_1) and breaking (d_2) bond lengths and the torsional dihedral angle (α) of a C−H bond of the methyl group with respect to the plane of the aromatic ring.

The geometries of the reactants, products, and TSs were optimized at various levels of theory.[57] Considering the TS geometry first, we see from Table 1 that, at all levels of theory, d_1 is modestly shorter than d_2 (average difference approximately 0.07 Å), which is consistent with a "late" (in the Hammond sense) TS and in accordance with the reaction endothermicity. The bond lengths d_1 and d_2 show a moderate dependence on the quantum chemical method used, which has also been noted in reports for other hydrogen-abstraction reactions.[23] For example, with the 6-31+G(d,p) basis set, values of d_1 range from 1.254 Å (MP2) to 1.325 Å (UHF), while values of d_2 range from 1.358 Å (RHF) to 1.398 Å (UMP2). There are also only modest differences associated with the choice of basis set, with 6-31+G(d,p) consistently producing TSs with somewhat shorter forming-bond and longer breaking-bond lengths than 6-31G(d). The method and basis set used for optimization does have a significant effect on the torsion angle α, with values ranging from about 15° to 30° (see Table 1). However, this is simply the result of an almost free rotor motion for the methyl group in the TS, with barriers to rotation of 0.1 kJ mol^{-1} or less.[58]

TABLE 1: Calculated Torsional Angle (α) and Forming (d_1) and Breaking (d_2) Bond Lengths in the Transition Structure for Hydrogen Abstraction from Benzene by Methyl Radical[a]

level of theory	α (°)	d_1 (Å)	d_2 (Å)
BP86/6-31G(d)	17.4	1.327	1.372
BP86/6-31+G(d,p)	15.5	1.311	1.388
BLYP/6-31G(d)	16.5	1.335	1.373
BLYP/6-31+G(d,p)	15.3	1.320	1.388
B3-P86/6-31G(d)	18.5	1.307	1.367
B3-P86/6-31+G(d,p)	15.7	1.294	1.379
B3-LYP/6-31G(d)	18.5	1.316	1.369
B3-LYP/6-31G(d,p)	16.7	1.313	1.371
B3-LYP/6-31+G(d,p)	15.2	1.304	1.382
B3-LYP/6-311G(d,p)	22.2	1.307	1.379
B3-PW91/6-31G(d)	16.4	1.310	1.368
B3-PW91/6-31+G(d,p)	16.7	1.298	1.380
MPW1K/6-31G(d)	16.0	1.296	1.363
MPW1K/6-31+G(d,p)	15.6	1.286	1.373
BB1K/6-31G(d)	17.4	1.304	1.355
BB1K/6-31+G(d,p)	16.5	1.294	1.365
MPWB1K/6-31G(d)	16.5	1.302	1.354
MPWB1K/6-31+G(d,p)	16.0	1.291	1.364
BMK/6-31G(d)	21.4	1.313	1.363
BMK/6-31+G(d,p)	21.5	1.302	1.375
UHF/6-31G(d)	30.1	1.332	1.360
UHF/6-31+G(d,p)	18.5	1.325	1.365
RHF/6-31G(d)	30.1	1.303	1.353
RHF/6-31+G(d,p)	30.1	1.298	1.358
MP2/6-31G(d)	30.2	1.274	1.385
MP2/6-31+G(d,p)	30.3	1.254	1.398
QCISD/6-31G(d)	31.4	1.310	1.370
QCISD/6-31+G(d,p)	30.3	1.292	1.372
CCSD/6-31G(d)	[b]	1.310	1.370
CCSD/6-31+G(d,p)	[b]	1.292	1.372
CCSD/6-311G(d,p)	[b]	1.296	1.374

[a] See Figure 1 for definitions of α, d_1, and d_2. [b] For the sake of computational efficiency, the CCSD optimizations were carried out with C_s symmetry, i.e., $\alpha = 0°$.

For the reactants and products, the effect of variation in theoretical procedure and basis set is generally similar in the closed-shell/radical pairs, i.e., methane/methyl radical and benzene/phenyl radical. An exception is found with the UMP2 structures for the phenyl radical. For example, the UMP2/6-31+G(d,p) values are 1.357 (C1−C2), 1.376 (C2−C3), and 1.373 (C3−C4) Å, significantly shorter than the BMK/6-31+G(d,p) values of 1.383 (C1−C2), 1.410 (C2−C3), and 1.403 (C3−C4) Å. In contrast, C−C bond lengths in benzene are very similar at the two levels: 1.399 (UMP2/6-31+G(d,p)) and 1.402 (BMK/6-31+G(d,p)) Å. The anomalous UMP2 results for the phenyl radical reflect the strong spin contamination in the UMP2/6-31+G(d,p) wave function ($\langle S^2\rangle = 1.230$).

The effect of the variation in optimized geometries on computed energies was assessed by performing single-point energy calculations on each structure at the URCCSD(T)/6-311+G(d,p) level of theory (see Figure 2). We can see that use of geometries optimized with either the 6-31G(d) or 6-31+G(d,p) basis set leads to very similar URCCSD(T) energies for virtually all the theoretical procedures. In addition, in the case of methyl radical and methane, the choice of the quantum chemical method used to optimize the geometry has little influence, leading to modest variations of less than 1.0 kJ

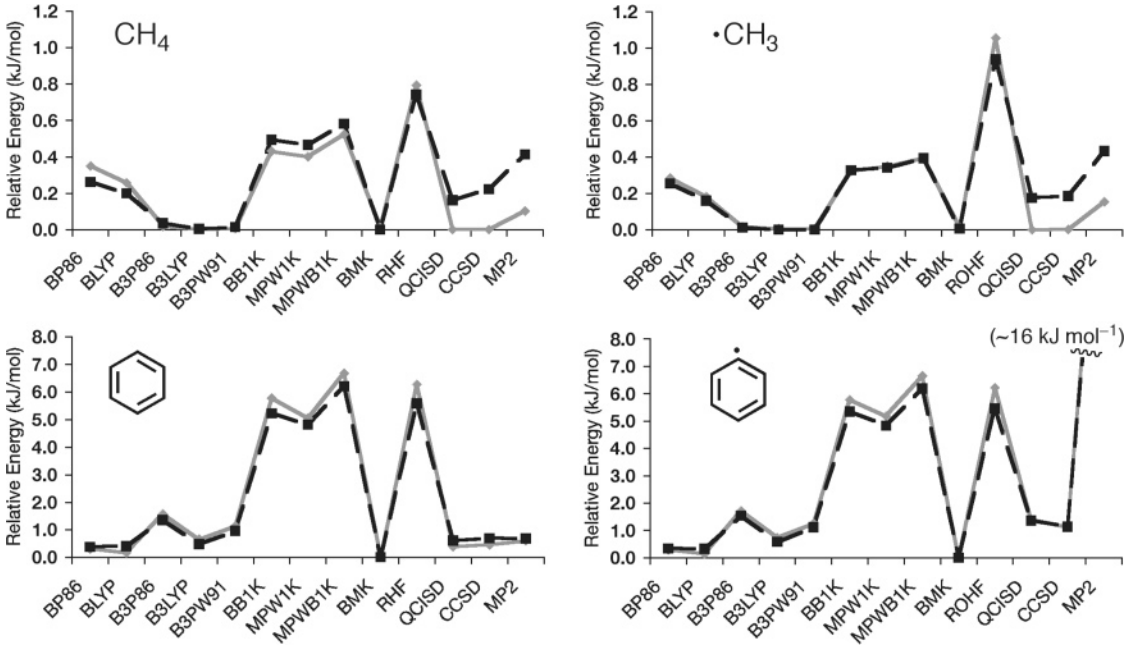

Figure 2. Variation in URCCSD(T)/6-311+G(d,p) total energies calculated for geometries optimized using a variety of levels of theory for methane, methyl radical, benzene, and phenyl radical. DFT, RHF, QCISD, CCSD, and MP2 methods were used in conjunction with the 6-31G(d) (solid gray line) and 6-31+G(d,p) (dashed black line) basis sets. The zero level is taken as the lowest energy obtained for a particular species with the particular basis set. The MP2 results for the heavily spin-contaminated phenyl radical are off-scale, with relative energies of approximately 16 kJ mol^{-1}, and are therefore not included.

mol^{-1} in the URCCSD(T) total energies. In contrast, the variations in total energies for benzene and the phenyl radical span ranges of ~7 and ~16 kJ mol^{-1}, respectively! If the UMP2 phenyl radical result is set aside, the results in Figure 2 show that the URCCSD(T) energy trends for the phenyl radical parallel those for benzene. The exceptional URCCSD(T)//UMP2 energy for the phenyl radical is associated with the effect on the UMP2-optimized geometry of the heavy spin contamination, as noted above. The large $\langle S^2 \rangle$ of the phenyl radical has been previously noted (UHF/6-31G(d) $\langle S^2 \rangle = 1.4$),[25] with the RCCSD(T) energy lying 9 kJ mol^{-1} below the UCCSD(T) value. Spin contamination is always a potential hazard in unrestricted descriptions of radical reactions.

The QCISD- and CCSD-optimized structures (in combination with the 6-31+G(d,p) basis set) for methane, methyl radical, and benzene are among the best on the URCCSD(T)/6-311+G-(d,p) surface, as also are the BMK structures (see Figure 2). BMK also produces the structure with the lowest URCCSD-(T)/6-311+G(d,p) energies for the phenyl radical, so it is clearly an attractive choice for optimizing the equilibrium structures in the benzene hydrogen-abstraction reaction. Figure 2 equally illustrates that the popular B3-LYP functional is also suitable for obtaining good geometries for stationary points of the studied reaction. BB1K and MPW1K are less good from this perspective.

When the URCCSD(T)/6-311+G(d,p) energies corresponding to the various optimized structures are used to calculate reaction enthalpies and barriers (Table 2), we see relatively little variation, indicating significant error cancellation. Geometries obtained with the DFT functionals, for example, lead to URCCSD(T) endothermicities that lie within the range 29.2 ± 0.2 kJ mol^{-1} and barriers of 78.5 ± 0.4 kJ mol^{-1}. The heavily spin-contamined (as indicated by the $\langle S^2 \rangle$ values of the transition structure and the phenyl radical) UHF, QCISD, and UCCSD geometries lead to endothermicities and barriers that lie somewhat below and above this range, respectively. The UMP2 geometries on the other hand show poor values for both the enthalpy and the barrier.

TABLE 2: Effect of Geometry on URCCSD(T)/6-311+G(d,p) Barriers (kJ mol^{-1}) and Reaction Enthalpies (kJ mol^{-1})

geometry	enthalpy[a]	barrier[a]	$\langle S^2 \rangle^b$	$\langle S^2 \rangle^c$
BP86/6-31G(d)	29.2	78.3	0.756	0.756
BP86/6-31+G(d,p)	29.1	78.4	0.755	0.756
BLYP/6-31G(d)	29.2	78.5	0.755	0.755
BLYP/6-31+G(d,p)	29.1	78.6	0.755	0.755
B3-P86/6-31G(d)	29.2	78.4	0.760	0.759
B3-P86/6-31+G(d,p)	29.3	78.5	0.759	0.759
B3-LYP/6-31G(d)	29.2	78.4	0.759	0.757
B3-LYP/6-31G(d,p)	29.2	78.4	0.759	0.757
B3-LYP/6-31+G(d,p)	29.3	78.5	0.759	0.757
B3-LYP/6-311G(d,p)	29.3	78.5	0.759	0.757
B3-PW91/6-31G(d)	29.2	78.1	0.760	0.760
B3-PW91/6-31+G(d,p)	29.3	78.5	0.760	0.760
MPW1K/6-31G(d)	29.3	78.9	0.770	0.769
MPW1K/6-31+G(d,p)	29.3	78.8	0.769	0.768
BB1K/6-31G(d)	29.2	78.5	0.763	0.762
BB1K/6-31+G(d,p)	29.4	78.7	0.763	0.761
MPWB1K/6-31G(d)	29.2	78.4	0.764	0.762
MPWB1K/6-31+G(d,p)	29.3	78.5	0.763	0.762
BMK/6-31G(d)	29.1	78.2	0.761	0.760
BMK/6-31+G(d,p)	29.1	78.3	0.761	0.760
UHF/6-31G(d)	24.8	73.9	1.423	1.433
UHF/6-31+G(d,p)	25.5	74.6	1.378	1.397
RHF/6-31G(d)	28.8	78.0	0.750	0.750
RHF/6-31+G(d,p)	28.8	78.0	0.750	0.750
UMP2/6-31G(d)	45.3	97.2	1.244	1.260
UMP2/6-31+G(d,p)	44.4	95.5	1.211	1.230
UQCISD/6-31G(d)	30.1	79.6	1.391	1.396
UQCISD/6-31+G(d,p)	29.9	79.2	1.354	1.366
UCCSD/6-31G(d)	29.8	79.2	1.399	1.402
UCCSD/6-31+G(d,p)	29.6	79.0	1.372	1.372
UCCSD/6-311G(d,p)	29.6	79.0	1.387	1.394

[a] Without ZPVE correction. [b] DFT or HF $\langle S^2 \rangle$ value in the transition structure, optimized at the theoretical level indicated. [c] DFT or HF $\langle S^2 \rangle$ value in the phenyl radical, optimized at the theoretical level indicated.

TABLE 3: Barriers ($\Delta E_0^{\ddagger}$) and Reaction Enthalpies (ΔH_{298}) for the Benzene Abstraction Reaction (kJ mol^{-1})

	B3-LYP geometry[a]		BMK geometry[b]	
method	ΔH_{298}	$\Delta E_0^{\ddagger}$	ΔH_{298}	$\Delta E_0^{\ddagger}$
G3-RAD [c]	35.4	72.5		
G3(MP2)-RAD[c]	37.1	73.8		
CBS-QB3[c]	42.1	77.6		
W1 (0 K)[c]	34.5	72.4[f]		
W1 (298 K)[c]	34.1			
BP86/6-31G(d)	17.3	37.8	17.3	38.2
B-LYP/6-31G(d)	18.5	45.2	18.5	45.6
B3-P86/6-31G(d)	22.6	51.4	22.5	51.6
UB3-LYP/6-31G(d)	23.4	57.8	23.3	58.1
B3-PW91/6-31G(d)	22.4	57.0	22.3	57.2
MPW1K/6-31G(d)	27.1	69.5	27.0	69.5
BB1K/6-31G(d)	21.7	64.4	21.6	64.5
MPWB1K/6-31G(d)	22.2	62.4	22.0	62.4
BMK/6-31G(d)	23.4	63.5	23.2	63.6
MPW1K/6-31+G(d,p)	33.4	73.0	33.3	73.0
BB1K/6-31+G(d,p)	28.5	69.4	28.4	69.4
BMK/6-31+G(d,p)	29.8	67.7	29.7	67.8
UB3-LYP/6-311+G(3df,2p)	30.5	66.2	30.0	66.8
RB3-LYP/6-311+G(3df,2p)	30.0	68.4	29.5	69.0
B3-PW91/6-311+G(3df,2p	28.7	63.0	28.3	63.6
MPW1PW91/6-311+G(3df,2p)	29.9	63.3	29.4	63.9
MPW1K/6-311+G(3df,2p)	33.4	74.1	33.3	74.1
BB1K/6-311+G(3df,2p)	28.7	71.0	28.6	71.0
MPWB1K/6-311+G(3df,2p)	29.2	69.1	28.7	69.6
BMK/6-311+G(3df,2p)	30.1	71.5	29.6	72.0
UHF/6-311+G(d,p)	17.5	113.6		
UMP2/6-311+G(d,p)	139.0	179.2		
UCCSD(T)/6-311+G(d,p)	42.4	82.9		
RHF/6-311+G(d,p)	42.7	156.3		
URCCSD(T)/6-311+G(d,p)	33.5	74.1		
UHF/6-311+G(3df,2p)	17.6	114.9	15.5	114.1
UMP2/6-311+G(3df,2p)	141.2	180.8	143.9	184.4
RHF/6-311+G(3df,2p)	41.4	156.5	40.7	156.8
RMP2/6-311+G(3df,2p)	38.8	63.2	38.3	63.3
URCCSD(T)/6-311+G(3df,2p)	33.8	72.9	33.2	73.4
expt (298 K)[d]	35.5			
Tokmakov et al. (0 K)[e]	36.8 ± 3.8			
G2M(CC,MP2) (0 K)[e]	43.1	81.9		

[a] B3-LYP/6-31+G(d,p) geometries, scaled ZPVEs, and thermal corrections, unless otherwise indicated. [b] BMK/6-31+G(d,p) geometries, scaled ZPVEs, and thermal corrections. [c] Geometries, ZPVEs, and thermal corrections as prescribed for these methods. [d] Calculated from experimental heats of formation from ref 60 (see text). [e] From ref 22. [f] See Note Added in Proof.

3.2. Reaction Enthalpies and Barriers. ΔH_{298} and $\Delta E_0^{\ddagger}$ values for the reaction between benzene and methyl radical were calculated using the B3-LYP/6-31+G(d,p) and BMK/6-31+G(d,p) geometries, using scaled ZPVEs and thermal corrections (Table 3).[56,59] A variety of methods were used in combination with the 6-31G(d), 6-31+G(d,p), and/or 6-311+G(3df,2p) basis sets to calculate energies. These include BP86, B-LYP, B3-P86, B3-LYP (U and R), B3-PW91, MPW1K, BB1K, MPWB1K, BMK, MPW1PW91, RMP2, and URCCSD(T). In addition, a selection of high-level composite procedures were employed, with the computationally demanding W1 method representing the highest-level procedure included in this study. Also included in Table 3 are the experimentally derived values of $\Delta H_{298} = 35.5$ kJ mol^{-1}, calculated using the 298 K enthalpies of formation of benzene (82.93 kJ mol^{-1}), methyl radical (145.69 kJ mol^{-1}), phenyl radical (339 kJ mol^{-1}), and methane (-74.87 kJ mol^{-1}),[60] and $\Delta H_0 = 36.8 \pm 3.8$ kJ mol^{-1}, calculated by Tokmakov et al.[22] using experimental C$-$H bond dissociation energies.

3.2.1. Reaction Enthalpies. The W1 procedure predicts a reaction enthalpy at 0 K of 34.5 kJ mol^{-1}, which is in close agreement with the experimental value reported by Tokmakov et al.[22] At 298 K, the W1 result amounts to 34.1 kJ mol^{-1}, though the good agreement with the experimental value (35.5 kJ mol^{-1}) might be somewhat fortuitous because of the considerable experimental uncertainty (± 8 kJ mol^{-1}) in the experimental $\Delta H_{f,298}$ for phenyl radical.[60] In light of this experimental uncertainty, the high-level W1 result will be treated as our benchmark value.[61] G3-RAD and G3(MP2)-RAD predict enthalpies in good agreement with the W1 value, with deviations of 1.3 and 3 kJ mol^{-1}, respectively. CBS-QB3 leads to a somewhat larger deviation (of 8 kJ mol^{-1}) from the W1 benchmark value, which may be associated with the spin contamination in the UMP2 wave function that is used in CBS-QB3 for the phenyl radical.[61] As previously noted, the dependence of reaction enthalpies on the level of theory used for the geometry optimization is limited, with very similar ΔH_{298} values being obtained for the B3-LYP and BMK geometries.

Inspection of the data resulting from standard DFT methods (Table 3) shows that there is a nonnegligible basis-set effect. The 6-31G(d) basis set appears to be too small to obtain accurate thermochemical data, significantly underestimating the ΔH_{298} W1 benchmark value. For example, inclusion of diffuse functions results in an improvement in the calculated MPW1K, BB1K, and BMK enthalpies by about 6$-$7 kJ mol^{-1}. However, a further upgrade to the larger 6-311+G(3df,2p) basis set has only a minor effect.

Of the noncomposite procedures, the computationally most expensive method, URCCSD(T)/6-311+G(3df,2p), performs the best, predicting a reaction enthalpy of 33.8 kJ mol^{-1} with the B3-LYP/6-31+G(d,p) geometry. URCCSD(T) performs quite well for the reaction enthalpy even with the more modest 6-311+G(d,p) basis set, giving 33.6 kJ mol^{-1} for B3-LYP/6-31+G(d,p) geometries.[62] RMP2 in combination with the 6-311+G(3df,2p) basis set (see Table 3) overestimates the W1 benchmark enthalpy by about 4$-$5 kJ mol^{-1},[63] whereas the large-basis-set DFT methods underestimate the benchmark enthalpy by 0.7$-$5.4 kJ mol^{-1}. The MPW1K functional gives a reaction enthalpy of 33.4 kJ mol^{-1}, in combination with both the 6-31+G(d,p) and 6-311+G(3df,2p) basis sets, which is very close to the benchmark result.

We note from Table 3 that UHF and particularly UMP2 produce poor values of the reaction enthalpy, both with the 6-311+G(d,p) and 6-311+G(3df,2p) basis sets. This is presumably associated with the high spin contamination in the product phenyl radical in the unrestricted wave functions. The UCCSD(T) reaction enthalpy appears to be in better agreement with our benchmark value but is still somewhat overestimated.[61]

3.2.2. Reaction Barriers. The $\Delta E_0^{\ddagger}$ values are also included in Table 3. Unfortunately, W1 calculations on the TS are computationally too demanding with our currently available resources (but see Note Added in Proof). In the absence also of reliable experimental information, the G3-RAD $\Delta E_0^{\ddagger}$ value of 72.5 kJ mol^{-1} is used as the benchmark for comparison of results from other methods. The choice of G3-RAD is supported by a recent extensive study of hydrocarbon hydrogen-abstraction reactions,[23] in which excellent agreement was found between G3X-RAD and W1, with an MAD of just 0.9 kJ mol^{-1}.[64] Most theoretical procedures underestimate the G3-RAD benchmark barrier, with the exception of MPW1K, which leads to surprisingly higher barriers when compared with similar DFT methods. The CBS-QB3 method also overestimates the benchmark value (by approximately 5 kJ mol^{-1}). A basis-set effect similar to that described for the reaction enthalpies is observed for the barriers. The average increase in barriers from 6-31G(d) to 6-31+G-

TABLE 4: Calculated Rate Constants at Various Temperatures (k_{600}, k_{700}, k_{800}; m^3 mol^{-1} s^{-1}), Activation Energies (E_a, kJ mol^{-1}), and Preexponential Factors (A, m^3 mol^{-1} s^{-1}) for the Benzene Abstraction Reaction ($C_6H_6 + \bullet CH_3 \rightarrow \bullet C_6H_5 + CH_4$) in the Temperature Range 600−800 K[a]

level[b]	k_{600}	k_{700}	k_{800}	E_a	A
BP86/6-31G(d)	4.64×10^3	1.61×10^4	4.10×10^4	43.5	2.84×10^7
BP86/6-31+G(d,p)	2.00×10^3	7.96×10^3	2.25×10^4	48.3	3.20×10^7
BLYP/6-31G(d)	1.13×10^3	4.73×10^3	1.39×10^4	50.1	2.59×10^7
BLYP/6-31+G(d,p)	3.41×10^2	1.71×10^3	5.74×10^3	56.3	2.72×10^7
B3-P86/6-31G(d)	3.03×10^2	1.49×10^3	4.94×10^3	55.7	2.14×10^7
B3-P86/6-31+G(d,p)	1.59×10^2	8.81×10^2	3.18×10^3	59.7	2.51×10^7
B3-LYP/6-31G(d)	8.37×10^1	4.87×10^2	1.82×10^3	61.5	1.89×10^7
B3-LYP/6-31+G(d,p)	3.14×10^1	2.15×10^2	9.07×10^2	67.1	2.18×10^7
B3-PW91/6-31G(d)	8.99×10^1	5.21×10^2	1.95×10^3	61.4	1.99×10^7
B3-PW91/6-31+G(d,p)	4.75×10^1	3.08×10^2	1.25×10^3	65.3	2.30×10^7
MPW1K/6-31G(d)	8.48×10^0	6.63×10^1	3.10×10^2	71.8	1.51×10^7
MPW1K/6-31+G(d,p)	4.95×10^0	4.30×10^1	2.18×10^2	75.5	1.85×10^7
BB1K/6-31G(d)	3.29×10^1	2.19×10^2	9.04×10^2	66.1	1.87×10^7
BB1K/6-31+G(d,p)	1.55×10^1	1.18×10^2	5.44×10^2	71.0	2.35×10^7
MPWB1K/6-31G(d)	3.64×10^1	2.35×10^2	9.49×10^2	65.1	1.69×10^7
MPWB1K/6-31+G(d,p)	1.67×10^1	1.25×10^2	5.64×10^2	70.2	2.16×10^7
BMK/6-31G(d)	3.04×10^1	2.05×10^2	8.56×10^2	66.6	1.91×10^7
BMK/6-31+G(d,p)	1.47×10^1	1.12×10^2	5.17×10^2	71.1	2.27×10^7
B3-LYP/6-311+G(3df,2p)[c]	1.98×10^1	1.45×10^2	6.48×10^2	69.6	2.27×10^7
BB1K/6-311+G(3df,2p)[c]	8.54×10^0	7.07×10^1	3.45×10^2	73.8	2.27×10^7
MPW1K/6-311+G(3df,2p)[c]	4.68×10^0	4.22×10^1	2.20×10^2	76.8	2.27×10^7
BMK/6-311+G(3df,2p)[c]	6.99×10^0	5.95×10^1	2.97×10^2	74.8	2.27×10^7
URCCSD(T)/6-311+G(3df,2p)[c]	5.38×10^0	4.76×10^1	2.44×10^2	76.1	2.27×10^7
CBS-QB3[d]	1.90×10^0	1.96×10^1	1.12×10^2	81.4	2.32×10^7
G3(MP2)-RAD[d]	3.82×10^0	3.45×10^1	1.80×10^2	76.9	1.89×10^7
G3-RAD[d]	4.96×10^0	4.32×10^1	2.19×10^2	75.6	1.89×10^7
exptl[e]			1.81×10^2	38.9	6.30×10^4
exptl[f]		3.95×10^1		63.0	1.99×10^6

[a] Calculated using the mixed harmonic oscillator and free rotor (HO/FR) model; see text. [b] Geometries, energies, and frequencies computed at the same theoretical level unless otherwise noted. [c] Calculated using BMK/6-31+G(d,p) geometries and frequencies. [d] Geometries, ZPVEs, and thermal corrections as prescribed for these methods. [e] Ref 26. [f] Ref 27.

(d,p) is now approximately 4 kJ mol^{-1}, while increasing the basis set to 6-311+G(3df,2p) results in an extra shift of about 2 kJ mol^{-1}.

Examination of the large-basis-set results in more detail shows that, as with the calculated enthalpies, the URCCSD(T)/6-311+G(3df,2p) barriers are in close agreement with the benchmark value, differing by less than 1 kJ mol^{-1}. However, the performance of RMP2 is less good, with a deviation of approximately 9 kJ mol^{-1} from the G3-RAD value, consistent with previous observations for radical additions to alkynes,[17] but in contrast to other studies on radical addition[16,17] and abstraction[23] reactions.

For the large-basis-set DFT results in Table 3, the deviations from the G3-RAD barrier lie between +1.6 and −9.5 kJ mol^{-1}. B3-LYP underestimates the barrier by about 6 kJ mol^{-1}. This is consistent with the results of Tokmakov et al.[22] and more general observations[32] that B3-LYP tends to underestimate reaction barriers. As found in other studies,[23] RB3-LYP shows a modest improvement over UB3-LYP, reducing the deviation from G3-RAD to about 4 kJ mol^{-1}. B3-PW91 and MPW1PW91 show deviations of about 9 kJ mol^{-1}, indicating that their good performance for the radical additions of methyl, ethyl, and propyl radicals to ethylene[65] cannot be generalized to the hydrogen-abstraction reactions for aromatic systems. MPWB1K, BB1K, and MPW1K, developed especially for kinetics applications, perform well. However, BMK shows the best performance of the DFT methods, giving barriers within 1 kJ mol^{-1} of the benchmark value.

Even more so than with the reaction enthalpy, UHF and UMP2 produce very poor values of the abstraction barrier, both with the 6-311+G(d,p) and 6-311+G(3df,2p) basis sets, leading to values that are substantially higher than our benchmark value (Table 3). In this case, presumably high spin contamination in the TS leads to problems with the unrestricted wave function. Interestingly, RHF also gives very high barriers. Clearly, these methods are not suitable for studying this and related reactions. UCCSD(T) leads to only a slight overestimation of the barrier compared with our benchmark value.[61]

3.3. Kinetic Parameters and Rate Constants. The kinetic parameters, i.e., the activation energy E_a and preexponential factor A, which were obtained by means of the HO/FR model in the relevant temperature range 600−800 K, are presented in Tables 4 and 5 for the forward ($C_6H_6 + \bullet CH_3 \rightarrow \bullet C_6H_5 + CH_4$) and reverse ($\bullet C_6H_5 + CH_4 \rightarrow C_6H_6 + \bullet CH_3$) reactions, respectively. The tabulated results include Eckart tunneling correction factors. A selection of methods was tested, in combination with the 6-31G(d), 6-31+G(d,p), and/or 6-311+G(3df,2p) basis sets. The rate constants at temperatures of 600, 700, and 800 K are also listed.

3.3.1. Tunneling Corrections. The predicted TST rate constants include Eckart quantum mechanical tunneling corrections, calculated in the experimentally relevant temperature range 600−800 K. For the sake of comparison, the Wigner method was also used to calculate the tunneling corrections. The calculated correction factors all lie between 1.2 and 2.2, with the Eckart corrections generally a little larger than the Wigner corrections (see Table S4 of the Supporting Information). As a result of the tunneling corrections, the activation energies decrease by approximately 5 kJ mol^{-1}, but the preexponential factors are influenced to a smaller extent. The rate curves that include tunneling experience a relatively small upward shift (rate increase) compared with the classical rate curves. Using the Eckart model, average corrections of 63% at 600 K and 36% at 800 K are found for the rate constants $k(T)$.

3.3.2. The HO vs HO/FR Model. Because the torsional frequency (ν_m) corresponding to the internal rotation of the

TABLE 5: Calculated Rate Constants at Various Temperatures (k_{600}, k_{700}, k_{800}; m^3 mol^{-1} s^{-1}), Activation Energies (E_a, kJ mol^{-1}), and Preexponential Factors (A, m^3 mol^{-1} s^{-1}) for the Reverse ($\bullet C_6H_5 + CH_4 \rightarrow C_6H_6 + \bullet CH_3$) Reaction in the Temperature Range 600−800 K[a]

level[b]	k_{600}	k_{700}	k_{800}	E_a	A
BP86/6-31G(d)	5.29×10^4	1.18×10^5	2.14×10^5	27.9	1.42×10^7
BP86/6-31+G(d,p)	5.42×10^4	1.19×10^5	2.16×10^5	27.6	1.37×10^7
BLYP/6-31G(d)	1.62×10^4	4.20×10^4	8.56×10^4	33.2	1.26×10^7
BLYP/6-31+G(d,p)	1.21×10^4	3.23×10^4	6.73×10^4	34.2	1.15×10^7
B3-P86/6-31G(d)	1.08×10^4	2.91×10^4	6.13×10^4	34.7	1.13×10^7
B3-P86/6-31+G(d,p)	1.37×10^4	3.58×10^4	7.34×10^4	33.5	1.13×10^7
B3-LYP/6-31G(d)	3.53×10^3	1.10×10^4	2.58×10^4	39.7	1.01×10^7
B3-LYP/6-31+G(d,p)	3.48×10^3	1.08×10^4	2.53×10^4	39.6	9.74×10^6
B3-PW91/6-31G(d)	3.13×10^3	1.00×10^4	2.39×10^4	40.6	1.07×10^7
B3-PW91/6-31+G(d,p)	4.02×10^3	1.24×10^4	2.87×10^4	39.2	1.04×10^7
MPW1K/6-31G(d)	8.33×10^2	3.11×10^3	8.35×10^3	46.0	8.42×10^6
MPW1K/6-31+G(d,p)	1.26×10^3	4.44×10^3	1.15×10^4	44.1	8.68×10^6
BB1K/6-31G(d)	8.21×10^2	3.14×10^3	8.57×10^3	46.8	9.74×10^6
BB1K/6-31+G(d,p)	1.04×10^3	3.85×10^3	1.03×10^4	45.7	9.89×10^6
MPWB1K/6-31G(d)	1.43×10^3	5.08×10^3	1.31×10^4	44.2	1.01×10^7
MPWB1K/6-31+G(d,p)	2.31×10^3	7.73×10^3	1.91×10^4	42.1	1.07×10^7
BMK/6-31G(d)	1.10×10^3	4.03×10^3	1.07×10^4	45.4	9.85×10^6
BMK/6-31+G(d,p)	1.43×10^3	5.05×10^3	1.30×10^4	44.1	9.86×10^6
B3-LYP/6-311+G(3df,2p)[c]	2.26×10^3	7.50×10^3	1.84×10^4	41.8	9.86×10^6
BB1K/6-311+G(3df,2p)[c]	7.37×10^2	2.86×10^3	7.93×10^3	47.4	9.86×10^6
MPW1K/6-311+G(3df,2p)[c]	1.02×10^3	3.77×10^3	1.01×10^4	45.8	9.86×10^6
BMK/6-311+G(3df,2p)[c]	7.37×10^2	2.86×10^3	7.93×10^3	47.4	9.86×10^6
URCCSD(T)/6-311+G(3df,2p)[c]	1.15×10^3	4.18×10^3	1.10×10^4	45.2	9.86×10^6
CBS-QB3[d]	2.38×10^3	7.93×10^3	1.96×10^4	42.0	1.08×10^7
G3(MP2)-RAD[d]	2.06×10^3	6.93×10^3	1.72×10^4	42.4	1.01×10^7
G3-RAD[d]	1.90×10^3	6.74×10^3	1.62×10^4	42.8	1.01×10^7
exptl[e]	1.96×10^2	8.57×10^2	2.59×10^3	51.6	6.03×10^6
exptl[f]	1.47×10^3	4.11×10^3	8.91×10^3	36.0	1.99×10^6
exptl[g]	7.22×10^1	2.72×10^2	7.38×10^2	46.4	7.90×10^5

[a] Calculated using mixed harmonic oscillator and free rotor (HO/FR) model; see text. [b] Geometries, energies, and frequencies computed at the same level unless otherwise noted. [c] Calculated using BMK/6-31+G(d,p) geometries and frequencies. [d] Geometries, ZPVEs, and thermal corrections as prescribed for these methods. [e] Ref 22. [f] Ref 28. [g] Ref 29.

methyl group is very small (ν_m lies in the range 3.4−45.1 cm^{-1}; see Table S5 of the Supporting Information), the harmonic oscillator approach is inappropriate, and the free rotor model should therefore be used for the description of this mode. We have compared E_a and A values for the benzene abstraction reaction, calculated using the HO and HO/FR models at a variety of levels of theory, and these results are also included in Table S5. The E_a values within the HO model are found to lie in the range 46.4−78.4 kJ mol^{-1}, whereas within the HO/FR model, the range of values is 43.5−81.4 kJ mol^{-1} (see also Table 4). In general, there is a decrease of about 3 kJ mol^{-1} when going from the HO to the HO/FR model, which is quite small compared with the 38 kJ mol^{-1} range of activation energies. This indicates the limited influence on the activation energy E_a of the method used for treating internal rotations (particularly when there is only one such motion), which is in accordance with previous findings.[6] In contrast, the preexponential factor varies significantly, with a difference of almost 1 order of magnitude depending on whether the rotation of the methyl group is handled using the HO/FR or HO model. The large variation in the torsional frequency (ν_m) calculated by the various levels of theory flows through to the HO predictions of the preexponential factor A (Table S5). This is not surprising in light of eq 2. However, this strong correlation between ν_m and A disappears when the methyl torsion is treated as a free rotor (HO/FR model). The preexponential factor now fluctuates within a small range of 1.5×10^7 to 3.2×10^7 m^3 mol^{-1} s^{-1} (Table 4). Only the results obtained with the HO/FR model are discussed in the remainder of this paper.

3.3.3. Experiment vs Theory. For the forward reaction, two experimental data sets are available, obtained by Krech and Price[26] and Zhang et al.[27] in the temperature intervals 744−800 K and 650−770 K, respectively. A large discrepancy exists between the kinetic parameters deduced from the two experiments (see Table 4), with respective activation energies of 38.9 and 63.0 kJ mol^{-1} and preexponential factors of 6.30×10^4 and 1.99×10^6 m^3 mol^{-1} s^{-1}. This is a clear example in which there are large uncertainties associated with the E_a and A values deduced from the experimental rate equation, that arise partly because the temperature range in which the experiments were carried out is quite narrow. This means that a large extrapolation is required to obtain the Arrhenius kinetic parameters. Under these circumstances, our high-level theoretical results are likely to serve as better benchmarks. The CBS-QB3, G3(MP2)-RAD, and G3-RAD values for E_a lie in the range 75−82 kJ mol^{-1}, while the values for A lie in the range $(1.9-2.3) \times 10^7$ m^3 mol^{-1} s^{-1}. Using these as benchmarks then suggests that BB1K, MPW1K, BMK, and URCCSD(T) in conjunction with the 6-311+G(3df,2p) basis set and using BMK/6-31+G(d,p) geometries and frequencies perform well.

The accuracy of the theoretical model can also be assessed by comparing directly the experimental and theoretical rate constants in the relevant temperature range. A first remark in this respect concerns the differences between the rate constants obtained in the two experiments in the overlapping temperature range 744−770 K. Remarkably, despite the substantial differences in the derived E_a and A values, the rate constants of Krech and Price[26] are only a factor of 1.5 larger than the rate constants obtained by Zhang et al.[27] The uncertainties in the measured rate constants are much smaller than for the kinetic parameters A and E_a because of the difficult extrapolation required to derive the latter. We find that the majority of the theoretical methods predict rate constants to within a factor of 10 of the two experimental rate curves in the entire temperature range.

TABLE 6: Calculated $\langle f_k \rangle$ Values for the Forward ($C_6H_6 + \bullet CH_3 \rightarrow \bullet C_6H_5 + CH_4$) and Reverse ($\bullet C_6H_5 + CH_4 \rightarrow C_6H_6 + \bullet CH_3$) Reactions[a]

	forward reaction		reverse reaction		
level[b]	ref 26	ref 27	ref 22	ref 28	ref 29
B3-P86/6-31G(d)	25.10	37.31	35.88	7.09	108.19
B3-P86/6-31+G(d,p)	15.83	22.14	44.38	8.73	133.35
B3-LYP/6-31G(d)	9.02	12.28	13.27	2.67	40.59
B3-LYP/6-31+G(d,p)	4.37	5.47	13.03	2.62	39.83
B3-PW91/6-31G(d)	9.64	13.15	12.00	2.42	36.80
B3-PW91/6-31+G(d,p)	6.09	7.83	14.92	3.00	45.58
MPW1K/6-31G(d)	1.46	1.71	3.67	0.76	11.42
MPW1K/6-31+G(d,p)	1.01	1.12	5.27	1.08	16.32
BB1K/6-31G(d)	4.37	5.56	3.69	0.76	11.51
BB1K/6-31+G(d,p)	2.57	3.05	4.54	0.93	14.12
MPWB1K/6-31G(d)	4.62	5.96	6.03	1.23	18.66
MPWB1K/6-31+G(d,p)	2.68	3.21	9.23	1.87	28.40
BMK/6-31G(d)	4.14	5.22	4.77	0.98	14.81
BMK/6-31+G(d,p)	2.45	2.89	5.99	1.22	18.54
B3-LYP/6-311+G(3df,2p)[c]	3.09	3.73	8.96	1.82	27.56
BB1K/6-311+G(3df,2p)[c]	1.61	1.83	3.37	0.70	10.51
MPW1K/6-311+G(3df,2p)[c]	1.01	1.10	4.45	0.92	13.84
BMK/6-311+G(3df,2p)[c]	1.38	1.55	3.37	0.70	10.51
URCCSD(T)/6-311+G(3df,2p)[c]	1.13	1.24	4.94	1.01	15.34
CBS-QB3[d]	0.51	0.52	9.48	1.92	29.16
G3(MP2)-RAD[d]	0.83	0.90	8.26	1.68	25.45
G3-RAD[d]	1.02	1.13	7.70	1.57	23.76

[a] f_k is defined as k_{theory}/k_{expt}. The $\langle f_k \rangle$ values tabulated here are average values calculated with respect to all the available relevant experimental data. [b] Geometries, frequencies, and energies computed at a single theoretical level unless otherwise noted. [c] Calculated using BMK/6-31+G(d,p) geometries and frequencies. [d] Geometries, ZPVEs, and thermal corrections as prescribed for these methods.

To quantify the deviations of the theoretical rate constants with respect to the experimental values, a factor $f_k = k_{theory}/k_{experiment}$ is introduced. A value of f_k greater than 1.0 indicates that theory is overestimating the rate constant compared with experiment. The calculated f_k values with respect to both available experiments are given in Table S6 of the Supporting Information. A schematic overview of the error analysis based on f_k values is given in Table 6. The numbers listed are the average values of f_k in the relevant temperature ranges (744−800 K for Krech and Price and 650−770 K for Zhang et al.). We can see that the composite methods such as G3(MP2)-RAD and G3-RAD perform extremely well in predicting the rate constants, with $\langle f_k \rangle$ values in the range 0.83−1.13. Also, the two-component method URCCSD(T)/6-311+G(3df,2p)//BMK, which uses the BMK/6-31+G(d,p) geometries and frequencies, has comparable accuracy. Among the DFT-based methods that use the same functional and basis for both the geometry and single-point energy calculations, MPW1K performs the best. The two-component methods that use BB1K, MPW1K, and BMK energies (obtained with the 6-311+G(3df,2p) basis set) and BMK/6-31+G(d,p) geometries and frequencies also give very good agreement with the experimental rates. The latter levels are also computationally extendable to larger systems such as polyaromatics and thus represent attractive cost-effective methods.

For the reverse reaction, results for three experiments are available, conducted by Tokmakov et al.,[22] Heckmann et al.,[28] and Duncan et al.,[29] in the temperature ranges 600−980, 560−1410, and 550−680 K, respectively. It can be seen (Table 5) that in this case there is significant variation among the experimental rate constants. The rate constants of Heckmann et al.[28] are larger than the values of Tokmakov et al.[22] values by a factor of approximately 5, whereas the data reported by Duncan et al.[29] are smaller than the values of Tokmakov et al. by a factor of about 3. The experimental analysis depends in many cases on the rates of various simultaneous side reactions, and therefore there is significant and unquantifiable uncertainty in the experimental rate constants.

The values of the f_k factors with respect to all three experiments are included in Table S7 of the Supporting Information, and an overview is given in Table 6. The calculated f_k values for our best methods (CBS-QB3, G3(MP2)-RAD, and G3-RAD) suggest that the experimental results of Heckmann et al.[28] are the most reliable. MPW1K/6-31+G(d,p) as well as BB1K, MPW1K, BMK, and CCSD(T) with the 6-311+G(3df,2p) basis set and BMK/6-31+G(d,p) geometries and frequencies all perform well, as in the case of the forward benzene abstraction reaction.

4. Conclusions

In the present study, the performance of a variety of theoretical procedures in predicting thermodynamic and kinetic parameters for the hydrogen-abstraction reaction between benzene and the methyl radical has been assessed, leading to the following broad conclusions.

(1) Very good geometries for methane, methyl radical, benzene, and phenyl radical are produced by BMK in combination with the 6-31G(d) and 6-31+G(d,p) basis sets. These geometries are in fact as good as or even better than their B3-LYP or CCSD counterparts. In general, the variations in the URCCSD(T)/6-311+G(d,p) single-point energies as a function of the level of theory used for geometry optimization are systematic, and as a consequence, there is significant error cancellation when evaluating the reaction enthalpy and barrier with structures of apparent lower quality. More specifically, the barriers and enthalpies calculated using high-level single points on lower-level optimized structures typically lie within a range of less than 1.6 kJ mol^{-1}. The exceptions are for comparisons involving UMP2-optimized structures for phenyl radical, which suffer from heavy spin contamination.

(2) Reaction enthalpies calculated with G3-RAD and URCCSD(T)/6-311+G(3df,2p) are in excellent agreement with the W1 benchmark value. The lower-level MPW1K results are also remarkably good. Other lower levels of theory, such as RMP2, B3-LYP, MPWB1K, and BMK, in combination with the 6-311+G(3df,2p) basis set, predict reasonable reaction enthalpies.

(3) The reaction barriers are more sensitive to the level of theory employed. The effect of the basis set is more pronounced, and the 6-31G(d) basis-set results reflect a significant basis-set error. Using the G3-RAD value of $\Delta E_0^{\ddagger}$ as the benchmark, we find that MPW1K, BB1K, and BMK perform very well. The URCCSD(T)/6-311+G(3df,2p) method predicts reaction barriers in very good agreement with G3-RAD.

(4) Activation energies and preexponential factors for both the forward ($C_6H_6 + \bullet CH_3 \rightarrow \bullet C_6H_5 + CH_4$) and reverse ($\bullet C_6H_5 + CH_4 \rightarrow C_6H_6 + \bullet CH_3$) reactions have been calculated in the temperature range 600−800 K. The computed activation energies cover a broad range in the case of the forward reaction. The influence on the calculated E_a of the method used for treating internal rotations is limited to 3 kJ mol^{-1}, whereas for the preexponential factor, there is a much greater sensitivity to this choice. On the other hand, the activation energy is much more sensitive than the preexponential factor to the level of theory used, with the latter being practically independent of this choice. In light of experimental uncertainties, the high-level methods CBS-QB3, G3(MP2)-RAD, and G3-RAD serve as

secondary benchmarks and indicate that good results are obtained from BB1K, MPW1K, and BMK energies (obtained with the 6-311+G(3df,2p) basis set) and BMK/6-31+G(d,p) geometries and frequencies.

(5) Finally, rate constants calculated for both the forward and reverse reactions reveal that a large proportion of our theoretical methods succeed in predicting rates that deviate by less than a factor of 10 from the experimental values. The functionals BMK, BB1K, and MPW1K, when used with a BMK/6-31+G(d,p) geometry, along with G3-RAD and G3(MP2)-RAD provide the best agreement with experiment. The inclusion of the Eckart tunneling correction reduces the E_a by a maximum of 5.3 kJ mol^{-1} and the preexponential factor by a factor of 0.6. The HO/FR model reduces E_a by a maximum of 2.9 kJ mol^{-1} and the A value by a factor of 0.2. Together, these two effects make a maximum contribution of 8 kJ mol^{-1} to the activation energies and a tenfold change in the preexponential factors for the benzene abstraction reaction.

Acknowledgment. K.H. wishes to thank Professor Leo Radom and members of his research group for their kind hospitality during her stay at the University of Sydney in January−May 2005, where this work originated. D.M. thanks the University of Sydney for a Sesqui Postdoctoral Fellowship. V.V.S. and M.W. thank the Fund for Scientific Research − Flanders, the Research Board of Ghent University. L.R. thanks the Australian Research Council for a Discovery Grant, and funding from the ARC Centre of Excellence in Free Radical Chemistry and Biotechnology, and gratefully acknowledges generous allocations of computing time from the Australian Partnership for Advanced Computing, the Australian National University Supercomputing Facility, and the Australian Centre for Advanced Computing and Communication. Finally, we thank Professor Jan Martin for making the BMK functional available for our use.

Note Added in Proof: Since submission of this paper, we have been able to calculate a W1 value for the benzene abstraction barrier. The result (72.4 kJ mol^{-1}) supports our use within the paper of the G3-RAD barrier (72.5 kJ mol^{-1}, Table 3) as the benchmark.

Supporting Information Available: Optimized geometries (Table S1), effect of DFT integration grid on barriers, enthalpies, activation energies and preexponential factors (Table S2), total energies, zero-point vibrational energies, and thermal corrections (Table S3), Wigner and Eckart tunneling correction factors (Table S4), effect of model used for handling the methyl rotation and effect of level of theory on activation energies and preexponential factors for the benzene abstraction reaction (Table S5), and detailed error analysis for the benzene abstraction reaction (Table S6) and the reverse reaction (Table S7). This material is available free of charge via the Internet at http://pubs.acs.org.

References and Notes

(1) Wauters, S.; Marin, G. B. *Chem. Eng. J.* **2001**, *82*, 267.

(2) Saeys, M.; Reyniers, M. F.; Marin, G. B.; Van Speybroeck, V.; Waroquier, M. *J. Phys. Chem. A* **2003**, *107*, 9147.

(3) Hemelsoet, K.; Van Speybroeck, V.; Marin, G. B.; De Proft, F.; Geerlings, P.; Waroquier, M. *J. Phys. Chem. A* **2004**, *108*, 7281.

(4) Saeys, M.; Reyniers, M. F.; Van Speybroeck, V.; Waroquier, M.; Marin, G. B. *ChemPhysChem* **2006**, *7*, 188.

(5) (a) Van Speybroeck, V.; Van Neck, D.; Waroquier, M.; Wauters, S.; Saeys, M.; Marin, G. B. *Int. J. Quantum Chem.* **2003**, *91*, 384. (b) Van Speybroeck, V.; Van Neck, D.; Waroquier, M.; Saeys, M.; Wauters, S.; Marin, G. B. *J. Phys. Chem. A* **2000**, *104*, 10939.

(6) Van Speybroeck, V.; Borremans, Y.; Van Neck, D.; Waroquier, M.; Wauters, S.; Saeys, M.; Marin, G. B. *J. Phys. Chem. A* **2001**, *105*, 7713.

(7) Van Speybroeck, V.; Reyniers, M. F.; Marin, G. B.; Waroquier, M. *ChemPhysChem* **2002**, *3*, 863.

(8) Van Speybroeck, V.; Hemelsoet, K.; Waroquier, M.; Marin, G. B. *Int. J. Quantum Chem.* **2004**, *96*, 568.

(9) Gonzales, J. M.; Barden, C. J.; Brown, S. T.; Schleyer, P. v. R.; Schaefer, H. F.; Li, Q.-S. *J. Am. Chem. Soc.* **2003**, *125*, 1064, and references therein.

(10) Watson, M. D.; Fechtenkötter, A.; Müllen, K. *Chem. Rev.* **2001**, *101*, 1267.

(11) (a) *Polycyclic Aromatic Hydrocarbons and Astrophysics*; Léger, A., d'Hendecourt, L., Boccara, N., Eds.; NATO ASI Series, Series C 191; Reidel: Dordrecht, 1987. (b) Puget, J. L.; Léger A. *Annu. Rev. Astron. Astrophys.* **1989**, *27*, 161.

(12) Pope, C. J.; Marr, J. A.; Howard, J. B. *J. Phys. Chem.* **1993**, *97*, 11001.

(13) Richter, H.; Mazyar, O. A.; Sumathi, R.; Green, W. H.; Howard, J. B.; Bozzelli, J. W. *J. Phys. Chem. A* **2001**, *105*, 1561.

(14) Harris, S. J.; Weiner, A. M.; Blint, R. J. *Combust. Flame* **1988**, *72*, 91.

(15) (a) Frenklach, M.; Clary, D. W.; Gardiner, W. C.; Stein, S. E. *Proc. Combust. Inst.* **1984**, *20*, 887. (b) Frenklach, M.; Warnatz, J. *Combust. Sci. Technol.* **1987**, *51*, 265. (c) Frenklach, M.; Wang, H. In *Proceedings of the 23rd International Symposium on Combustion*; The Combustion Institute: Pittsburgh, PA, 1990; p 1559. (d) Frenklach, M. In *Proceedings of the 23rd International Symposium on Combustion*; The Combustion Institute: Pittsburgh, PA, 1996; p 2258.

(16) (a) Coote, M. L.; Wood, G. P. F.; Radom, L. *J. Phys. Chem. A* **2002**, *106*, 12124. (b) Gómez-Balderas, R.; Coote, M. L.; Henry, D. J.; Fischer, H.; Radom, L. *J. Phys. Chem. A* **2003**, *107*, 6082. (c) Henry, D. J.; Coote, M. L.; Gómez-Balderas, R.; Radom, L. *J. Am. Chem. Soc*. **2004**, *126*, 1732.

(17) Gómez-Balderas, R.; Coote, M. L.; Henry, D. J.; Radom, L. *J. Phys. Chem. A* **2004**, *108*, 2874.

(18) Saeys, M.; Reyniers, M. F.; Marin, G. B.; Van Speybroeck, V.; Waroquier, M. *AIChE J.* **2004**, *50*, 426.

(19) For a recent comprehensive review, see: Fischer, H.; Radom, L. *Angew. Chem., Int. Ed.* **2001**, *40*, 1340.

(20) (a) Basch, H.; Hoz, S. *J. Phys. Chem. A* **1997**, *101*, 4416. (b) Jursic, B. S. *Chem. Phys. Lett.* **1997**, *264*, 113. (c) Schimmel, P. H. A.; Ruttink, P. J. A.; de Jong, B. H. W. S. *J. Phys. Chem. B* **1999**, *103*, 10506. (d) Pu, J.; Truhlar, D. G. *J. Phys. Chem. A* **2005**, *109*, 773. (e) Lynch, B. J.; Fast, P. L.; Harris, M.; Truhlar, D. G. *J. Phys. Chem. A* **2000**, *104*, 4811. (f) Kang, J. K.; Musgrave, C. B. *J. Chem. Phys.* **2001**, *115*, 11040.

(21) Lynch, B. J.; Truhlar, D. G. *J. Phys. Chem. A* **2001**, *105*, 2936.

(22) Tokmakov, I. V.; Park, J.; Gheyas, S.; Lin, M. C. *J. Phys. Chem. A* **1999**, *103*, 3636.

(23) Coote, M. L. *J. Phys. Chem. A* **2004**, *108*, 3865.

(24) Mebel, A. M.; Lin, M. C.; Yu, T.; Morokuma, K. *J. Phys. Chem. A* **1997**, *101*, 3189.

(25) Nicolaides, A.; Smith, D. M.; Jensen, F.; Radom, L. *J. Am. Chem. Soc.* **1997**, *119*, 8083.

(26) Krech, M.; Price, S. J. W. *Can. J. Chem.* **1967**, *45*, 157.

(27) Zhang, H. X.; Ahonkhai, S. I.; Back, M. H. *Can. J. Chem.* **1989**, *67*, 1541.

(28) Heckmann, E.; Hippler, H.; Troe, J. *Symp. Int. Combust. Proc.* **1996**, *16*, 543.

(29) Duncan, F. J.; Trotman-Dickenson, A. F. *J. Chem. Soc.* **1962,** *52*, 4672.

(30) Kohn, W.; Becke, A. D.; Parr, R. G. *J. Phys. Chem.* **1996**, *100*, 12974.

(31) Becke, A. D. *J. Chem. Phys.* **1993**, *98*, 5648.

(32) Van Speybroeck, V.; De Kimpe, N.; Waroquier, M. *J. Org. Chem.* **2005**, *70*, 3674.

(33) Lingwood, M.; Hammond, J. R.; Hrovat, D. A.; Mayer, J. M.; Borden, W. T. *J. Chem. Theory Comput.* **2006**, *2*, 740.

(34) Boese, A. D.; Martin, J. M. L. *J. Chem. Phys.* **2004**, *121*, 3405.

(35) Zhao, Y.; Truhlar, D. G. *J. Phys. Chem. A* **2004**, *108*, 6908.

(36) Zhao, Y.; Lynch, B. J.; Truhlar, D. G. *Phys. Chem. Chem. Phys.* **2005**, *7*, 43.

(37) Zhao, Y.; González-García, N.; Truhlar, D. G. *J. Phys. Chem. A* **2005**, *109*, 2012.

(38) (a) Hehre, W. J.; Radom, L.; Schleyer, P. v. R.; Pople, J. A. *Ab Initio Molecular Orbital Theory*; Wiley: New York, 1986. (b) Jensen, F. *Introduction to Computational Chemistry*; Wiley: New York, 1999.

(39) Koch, W.; Holthausen, M. C. *A Chemist's Guide to Density Functional Theory*; Wiley-VCH: Weinheim, 2000.

(40) Frisch, M. J.; Trucks, G. W.; Schlegel, H. B.; Scuseria, G. E.; Robb, M. A.; Cheeseman, J. R.; Montgomery, J., J. A.; Vreven, T.; Kudin, K. N.;

Burant, J. C.; Millam, J. M.; Iyengar, S. S.; Tomasi, J.; Barone, V.; Mennucci, B.; Cossi, M.; Scalmani, G.; Rega, N.; Petersson, G. A.; Nakatsuji, H.; Hada, M.; Ehara, M.; Toyota, K.; Fukuda, R.; Hasegawa, J.; Ishida, M.; Nakajima, T.; Honda, Y.; Kitao, O.; Nakai, H.; Klene, M.; Li, X.; Knox, J. E.; Hratchian, H. P.; Cross, J. B.; Bakken, V.; Adamo, C.; Jaramillo, J.; Gomperts, R.; Stratmann, R. E.; Yazyev, O.; Austin, A. J.; Cammi, R.; Pomelli, C.; Ochterski, J. W.; Ayala, P. Y.; Morokuma, K.; Voth, G. A.; Salvador, P.; Dannenberg, J. J.; Zakrzewski, V. G.; Dapprich, S.; Daniels, A. D.; Strain, M. C.; Farkas, O.; Malick, D. K.; Rabuck, A. D.; Raghavachari, K.; Foresman, J. B.; Ortiz, J. V.; Cui, Q.; Baboul, A. G.; Clifford, S.; Cioslowski, J.; Stefanov, B. B.; Liu, G.; Liashenko, A.; Piskorz, P.; Komaromi, I.; Martin, R. L.; Fox, D. J.; Keith, T.; Al-Laham, M. A.; Peng, C. Y.; Nanayakkara, A.; Challacombe, M.; Gill, P. M. W.; Johnson, B.; Chen, W.; Wong, M. W.; Gonzalez, C.; Pople, J. A. *Gaussian 03*, revision C2; Gaussian, Inc.: Wallingford, CT, 2004.

(41) Werner, H.-J.; Knowles, P. J.; Amos, R. D.; Bernhardsson, A.; Berning, A.; Celani, P.; Cooper, D. L.; Deegan, M. J. O.; Dobbyn, A. J.; Eckert, F.; Hampel, C.; Hetzer, G.; Korona, T.; Lindh, R.; Lloyd, A. W.; McNicholas, S. J.; Manby, F. R.; Meyer, W.; Mura, M. E.; Nicklass, A.; Palmieri, P.; Pitzer, R.; Rauhut, G.; Schütz, M.; Stoll, H.; Stone, A. J.; Tarroni, R.; Thorsteinsson, T. *MOLPRO 2000.6*; University of Birmingham: Birmingham, U. K., 1999.

(42) Stanton, J. F.; Gauss, J.; Watts, J. D.; Nooijen, M.; Oliphant, N.; Perera, S. A.; Szalay, P. G.; Lauderdale, W. J.; Kucharski, S. A.; Gwaltney, S. R.; Beck, S.; Balková, A.; Bernholdt, D. E.; Baeck, K. K.; Rozyczko, P.; Sekino, H.; Hober, C.; Bartlett, R. J. *ACES II*; Quantum Theory Project; University of Florida: Gainsville, FL, 2005.

(43) (a) Ochterski, J. W.; Petersson, G. A.; Montgomery, J. A. *J. Chem. Phys.* **1996**, *104*, 2598. (b) Montgomery, J. A.; Frisch, M. J.; Ochterski, J. W.; Petersson, G. A. *J. Chem. Phys.* **2000**, *112*, 6532.

(44) Henry, D. J.; Parkinson, C. J.; Mayer, P. M.; Radom, L. *J. Phys. Chem. A* **2001**, *105*, 6750.

(45) (a) Henry, D. J.; Sullivan, M. B.; Radom, L. *J. Chem. Phys.* **2003**, *118*, 4849. (b) Henry, D. J.; Parkinson, C. J.; Radom, L. *J. Phys. Chem. A* **2002**, *106*, 7927.

(46) Martin, J. M. L.; Parthiban, S. In *Quantum Mechanical Prediction of Thermochemical Data*; Cioslowski, J., Ed.; Kluwer-Academic: Dordrecht, The Netherlands, 2001; pp 31−65.

(47) (a) Wynne-Jones, W. F. K.; Eyring, H. J. *J. Chem. Phys.* **1936**, *3*, 492. (b) Evans, M. G.; Polanyi, M. *Trans. Faraday Soc.* **1935**, *31*, 875. (c) Evans, M. G.; Polanyi, M. *Trans. Faraday Soc.* **1937**, *33*, 448.

(48) (a) Laidler, K. J. *Chemical Kinetics*; HarperCollins: New York, 1987. (b) McQuarrie D. A.; Simon, J. D. *Physical Chemistry − A Molecular Approach*; University Science Books: Sausalito, CA, 1997.

(49) Wigner, E. *J. Chem. Phys.* **1937**, *5*, 720.

(50) Eckart, C. *Phys. Rev.* **1930**, *35*, 1303.

(51) Truong, T. N.; Duncan, W. T.; Tirtowidjojo, M. *Phys. Chem. Chem. Phys.* **1999**, *1*, 1061, and references herein.

(52) Troe, J. *J. Chem. Phys.* **1977**, *66*, 4758.

(53) Van Cauter, K.; Van Speybroeck, V.; Vansteenkiste, P.; Reyniers, M. F.; Waroquier, M. *ChemPhysChem* **2006**, *7*, 131.

(54) Scott, A. P.; Radom, L. *J. Phys. Chem.* **1996**, *100*, 16502.

(55) Zhao, Y.; Lynch, B. J.; Truhlar, D. G. *J. Phys. Chem. A* **2004**, *108*, 2715.

(56) Values used in the present study for B3-LYP/6-31+G(d,p) are 0.9806 (ZPVE) and 0.9989 ($\Delta\Delta H$), while for BMK/6-31+G(d,p), they are 0.95 (ZPVE) and 0.98 ($\Delta\Delta H$).

(57) Geometries of reactants and products at the B3-LYP/6-31+G(d,p), BMK/6-31+G(d,p), and CCSD/6-31+G(d,p) levels are presented in Table S1.

(58) Since the rotation of the methyl group in the TS has a very low frequency, the effect of the DFT integration grid on the value of the computed frequencies was checked using the B3-LYP and BP86 functionals. However, as shown in Table S2, the results are independent of the integration grid used.

(59) The component absolute energies, ZPVEs, and thermal corrections are presented in Table S3 of the Supporting Information.

(60) http://webbook.nist.gov/chemistry.

(61) We note that W1 is based on the URCCSD(T) procedure of MOLPRO, as is G3-RAD and G3(MP2)-RAD. CBS-QB3, on the other hand, is based on the fully unrestricted UMP2 and UCCSD(T) procedures of Gaussian, together with a spin correction. The comparison of results among the various methods partly reflects this unrestricted/restricted treatment. The experimental reaction enthalpy values lie between those based on URCCSD(T) and those based on spin-corrected UCCSD(T) but are closer to the former.

(62) Calculated from the vibrationless enthalpy in Table 2 and the ZPVE and $\Delta\Delta H$ corrections in Table S3 of the Supporting Information.

(63) We note that RMP2/6-31G(d,p) calculations lead to an enthalpy value of 34.6 kJ mol^{-1}, very close to the experimental value.

(64) For molecules containing only first-row elements, G3-RAD and G3X-RAD only differ in the choice of geometry and would give identical results in the present study (where prescribed geometries are used).

(65) Van Speybroeck, V.; Van Cauter, K.; Coussens, B.; Waroquier, M. *ChemPhysChem* **2005**, *6*, 180.